SAGE CRISP PUBLICATIONS DIRECTORY

Authors:-

Powrie, W. and Li, E.S.F.

FINITE ELEMENT ANALYSES OF AN IN SITU WALL PROPPED AT FORMATION LEVEL,

Publication:-

GEOTECHNIQUE,
VOL 41, NO.4,pp 499-514

Year of Publication:-

1991

Powrie, W. & Li, E. S. F. (1991). *Géotechnique* 41, No. 4, 499–514

Finite element analyses of an in situ wall propped at formation level

W. POWRIE* and E. S. F. LI†

The use of formation-level props to support an in situ retaining wall can result in a structural system which is stiff and remote from rotational failure. However, the interaction between the wall, the soil and a continuous prop slab cannot be analysed using simple techniques. Finite element analyses have been carried out to investigate some of the factors affecting the behaviour of an in situ wall, propped at formation level, retaining 9 m of stiff overconsolidated boulder clay. This Paper describes the results of a parametric study in which the effects of soil/wall/prop stiffness and the pre-excavation earth pressure coefficient were investigated. It is found that, because the wall is very stiff, computed deformations are governed by the assumed stiffness of the soil rather than the flexural rigidity of the wall. Bending moments in the wall are influenced significantly by the assumed pre-excavation lateral earth pressures and, to a lesser extent, by the nature of the structural connection between the wall and the permanent prop slab.

KEYWORDS: clays; diaphragm and in situ walls; numerical modelling and analysis; retaining walls; soil/structure interaction.

L'emploi d'étais mis en place lors de la construction pour conforter un mur de soutènement en place peut produire un système structural rigide et peu sujet à la rupture circulaire. Il est cependant impossible d'analyser à l'aide de techniques simples l'interaction entre le mur, le sol et et une semelle d'appui continue. Des analyses a' éléments finis ont été effectuées pour étudier quelques-uns des facteurs qui influencent le comportement d'un mur en place étayé en cours de construction qui retient 9 m d'argile à blocaux rigide surconsolidée. L'article décrit les résultats d'une étude paramétrique pour examiner les effets de la rigidité sol/mur/support et du coefficient de poussée des terres avant l'excavation. On a trouvé qu'en raison de la rigidité élevée du mur les déformations calculées sont regies par la rigidité admise du sol plutôt que par la rigidité en flexion du mur. Les moments de flexion dans le mur sont affectés de facon significative par les pressions latérales admises des terres avant l'excavation et aussi à un moindre degré par la nature du rapport structural entre le mur et la semelle d'appui permanente.

INTRODUCTION

In situ methods of retaining wall construction have been popular for at least a decade, particularly where the land available for temporary works activities is limited. Such walls generally act as embedded cantilevers, sometimes supported by props at one or more levels. Designs incorporating a single level of props at excavation level have recently become more common, often in connection with underpasses for urban road improvement schemes.

Considerable economic benefits can result from the use of a permanent prop at formation level, as the depth of embedment required to prevent rotational failure is comparatively small. The design depth of embedment, however, may well be governed by the need to prevent excessive deformation during excavation to formation level with temporary props in place, before the permanent props are installed. Once the permanent props are in place, the resulting structural system will be comparatively stiff, and—depending on the initial in situ lateral earth pressure and the disturbance resulting from the installation and construction of the wall—the lateral stresses in the retained soil may be high (Symons & Carder, 1989). For a road, the permanent prop might be in the form of a continuous slab, which would tend to resist heave at the excavated soil surface. The resulting interaction between the soil, the wall and the permanent prop slab might be difficult to quantify.

This Paper describes a series of analyses using the finite element program CRISP (Britto & Gunn, 1987), to investigate the influence of various factors on the behaviour of an in situ wall propped at formation level. The wall analysed retains one side of a 9 m deep cutting through stiff, overconsolidated boulder clay, underlain at a

Discussion on this Paper closes 1 April 1992; for further details see p. ii.

* Department of Civil Engineering, Queen Mary and Westfield College (University of London).
† Sir Alexander Gibb & Partners.

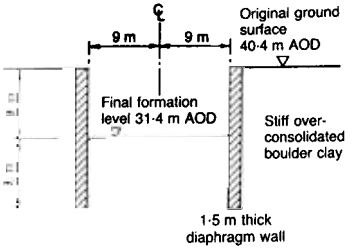

Fig. 1. Idealized cross-section

depth of 40 m by stiff rock. The idealized geometry is shown in Fig. 1.

SOIL MODEL

For the analyses described in this Paper, a finite element formulation of a soil model proposed by Schofield (1980) was used. This model incorporates the Cam clay yield surface on the wet side of the critical state, and the Hvorslev surface and a no-tension cut-off on the dry side (Fig. 2(a)). The Hvorslev surface and the no-tension cut-off are used in preference to the Cam clay yield surface on the dry side of the critical state because of the overestimation of the elastic response of soils on the dry side by conventional Cam clay models. In the finite element formulation, the Hvorslev surface and the no-tension cut-off are treated as yield surfaces, which govern the direction of the plastic strain increment vector due to the assumption in CRISP of associated flow—i.e. the plastic potential (to which plastic strain increment vectors are normal) and the yield surface coincide.

Although in reality soils may not dilate strongly enough for normality to be applicable to the Hvorslev surface and the no-tension cut-off, the finite element formulation of the Schofield model was used successfully by Bolton, Britto, Powrie & White (1989) to replicate rupture patterns observed in front of a centrifuge model wall retaining overconsolidated kaolin. In the analyses described in this Paper, the stress ratios q/p' were generally well within the specified yield surface, and the results would not have been significantly different if a conventional Cam clay model had been used.

For overconsolidated soils remote from failure, the elastic stiffness of each element is calculated from the slope κ of the unload/reload lines in v–ln p' space

$$E' = 3(1 - 2\nu')vp'/\kappa \tag{1}$$

$$v = (1 + e) = (1 + e_0 + \lambda - \kappa) - \lambda \ln p'_{max} + \kappa \ln [p'_{max}/p'] \tag{2}$$

where E' is the effective stress Young's modulus, ν' is the effective stress Poisson's ratio, v is the specific volume, p' is the average effective stress, e is the void ratio, e_0 is the void ratio on critical state line at $p' = 1$ kPa, and λ is the slope of critical state line in v–ln p space (see Table 1 and Fig. 2b).

SOIL PARAMETERS

The soil parameters used in the analysis are summarized in Table 1. These are based mainly on laboratory and in situ test data on stiff overconsolidated boulder clay, as described by Li (1990).

While λ, κ and e_0 should strictly be determined in isotropic compression and swelling, it is considered that the use of oedometer test data will not introduce any significant error. The stress history of the deposit was assumed to comprise

Table 1. Soil parameters used in the analysis (case 1)

Soil parameters (Schofield model)	
Slope of one-dimensional compression line in v–ln p' space	$\lambda = 0{\cdot}155$
Slope of unload/reload line in v–ln p' space	$\kappa = 0{\cdot}016$
Specific volume (and void ratio) on critical state line at $p' = 1$ kPa in v–ln p' space	$\Gamma = 2{\cdot}41$ ($e_0 = 1{\cdot}41$)
Slope of critical state line in q–p' space	$M = 1{\cdot}03$
Poisson's ratio	$\nu' = 0{\cdot}2$
Unit weight of water	$\gamma_w = 9{\cdot}81$ kN/m^3
Bulk unit weight of soil	$\gamma = 22{\cdot}0$ kN/m^3
Permeability in vertical direction	$k_v = 10^{-10}$ m/s
Permeability in horizontal direction	$k_h = 10^{-10}$ m/s
Angle of Hvorslev surface in τ–σ' space	$\phi_H = 15{\cdot}5°$
Slope of no-tension cut-off in q–p' space	$S = 2{\cdot}0$
Permeability in vertical direction for tensile fracture region	$k_v = 10^{-6}$ m/s
Permeability in horizontal direction for tensile fracture region	$k_h = 10^{-6}$ m/s

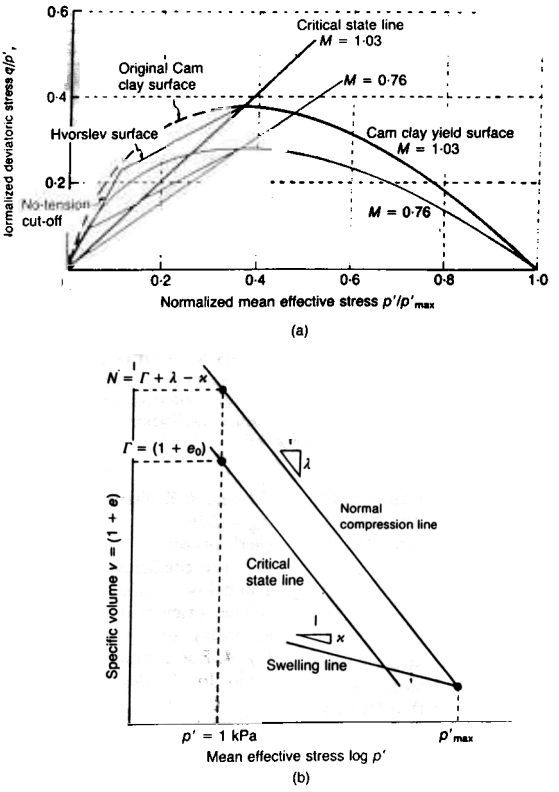

Fig. 2. (a) Cam clay yield surface, Hvorslev surface and no-tension cut-off in normalized q–p' space; (b) Cam clay model in v–log p' space

one-dimensional consolidation followed by the removal of an effective overburden pressure of 2500 kPa: the overconsolidation ratio (OCR) based on σ_v' is given as a function of depth in Table 2. Fig. 3 compares the idealized Cam clay model based on the parameter values used in the analysis ($\lambda = 0{\cdot}155$, $\kappa = 0{\cdot}016$, $e_0 = 1{\cdot}41$) with data from oedometer tests on overconsolidated boulder clay.

The slope of the line joining critical states in $q : p'$ space was taken as $M = 1{\cdot}03$. This was based on a critical state angle of shearing resistance $\phi'_{crit} = 26°$ measured in drained triaxial compression. If the stress ratio q/p' at the critical state is assumed to be constant, the implied angle of shearing resistance in the plane containing the major and minor principal effective stresses ϕ_{13}' depends on the magnitude of the intermediate principal effective stress σ_2', and the adoption of $M = 1{\cdot}03$ might lead to an unrealistically high value of ϕ_{13}' in plane strain. However, the present analysis is substantially insensitive to the value chosen for M because the soil is generally remote from the critical stress ratio. When the analysis was repeated with $M = 0{\cdot}76$ (giving $\phi_{13}' = 26°$ when $\sigma_2' = \frac{1}{2}[\sigma_1' + \sigma_3']$, which is often taken to correspond approximately to plane strain conditions), the difference in the results was insignificant.

The slope H of the Hvorslev surface along a constant volume line in q–p' space was taken to be 0·6; the slope S of the no-tension cut-off was taken to be 2. Repetition of the analysis with $S = 3$ produced no discernible difference in the results, because few elements were close to this part of the failure envelope.

The permeability of the boulder clay was taken as 10^{-10} m/s, except in regions affected by tensile fracture in which an increase in permeability of a factor of 10 000 was assumed. The latter is purely

Table 2. In situ and pre-excavation stress states*

1	2	3	4	5	6	7	8	9
0·0	0·0	0·0	—	2·56	1·0	0·0	2·0	0·0
1·0	0·0	22·0	114·6	2·56	1·0	22·0	2·0	44·0
2·0	9·8	34·2	74·1	2·56	1·0	34·2	2·0	68·4
4·0	29·4	58·6	43·7	2·56	1·0	58·6	2·0	117·2
9·0	78·4	119·6	21·9	2·17	1·0	119·6	2·0	239·2
14·0	127·4	180·6	14·8	1·83	1·0	180·6	1·83	330·5
18·0	166·6	229·4	11·9	1·66	1·0	229·4	1·66	380·8
18·9	175·4	240·4	11·4	1·63	1·63	392·5	1·63	392·5
25·0	235·2	314·8	8·9	1·46	1·46	461·0	1·46	461·0
32·0	303·8	400·2	7·2	1·34	1·34	537·3	1·34	537·3
40·4	386·1	502·7	6·0	1·23	1·23	619·3	1·23	619·3

* Column 1: Depth below original ground level: m. Column 2: Pore water pressure: kPa. Column 3: Vertical effective stress: kPa. Column 4: Overconsolidation ratio based on vertical effective stresses. Column 5: Initial in situ lateral earth pressure coefficient, equation (3). Column 6: Pre-excavation lateral earth pressure coefficient, case 1. Column 7: Pre-excavation lateral effective stress, case 1: kPa. Column 8: Pre-excavation lateral earth pressure coefficient, case 2. Column 9: Pre-excavation lateral effective stress, case 2: kPa.

conjectural, but did not feature significantly in the analysis. The unit weight of the soil was taken to be 22 kN/m^3; Poisson's ratio was taken to be 0·2 (Stroud & Butler, 1975).

IN SITU STRESS STATE AND SOIL STIFFNESS PROFILE

The initial in situ lateral effective stresses were estimated from the assumed stress history (i.e. the removal of 2500 kPa of effective overburden) and the expression

$$K_0 = \sigma_h'/\sigma_v' = (1 - \sin \phi') \, \mathrm{OCR}^{\sin \phi'} \qquad (3)$$

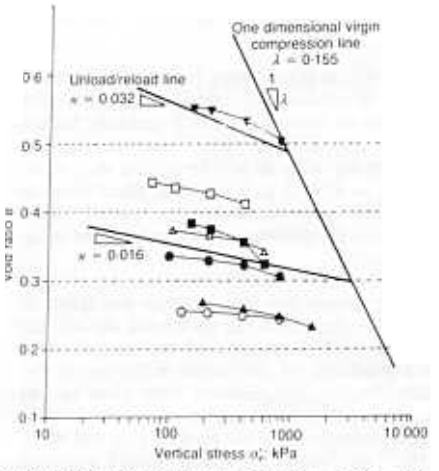

Fig. 3. Oedometer test data, Cam clay model and parameters

(Mayne & Kulhawy, 1982), up to the passive limit $K_p = 2{\cdot}56$ for $\phi' = 26°$ (K_0 is the initial in situ earth pressure coefficient, K_p is the passive earth pressure coefficient). The water table was set at 1 m below original ground level.

The calculated in situ soil stiffness profile according to equations (1) and (2) is shown in Fig. 4. For comparison, soil stiffness values measured for boulder clay tested in conventional drained triaxial compression (secant moduli at 1% axial strain), undrained triaxial compression

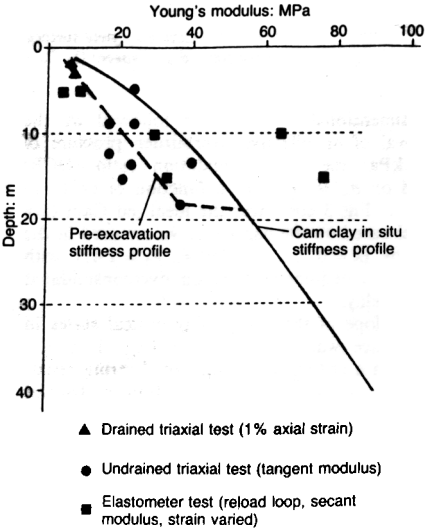

Fig. 4. Computed and measured soil stiffness

(initial tangent moduli assuming $\nu' = 0{\cdot}2$ and $\nu_u = 0{\cdot}5$), and in situ using a type of pressuremeter (secant moduli on reloading) are also shown. The relevance of these experimental stiffness values depends on their having been measured in an appropriate stress path and at an appropriate strain level.

The finite element analysis started with the wall already in place, so that only the changes in stress and strain which occurred after installation of the wall were investigated. The initial in situ lateral stresses were therefore modified in an attempt to take account of the stress reduction which installation of the wall might cause. This is a complex problem, as the effects of wall installation depend on a number of factors including the method of wall construction (e.g. using rectangular panels or circular piles) and the relative timescale of excess pore water pressure dissipation in the soil. For the main analysis, it was assumed that the effects of wall installation could be represented by reducing the lateral earth pressure coefficient (based on effective stresses) to unity in the soil above the toe of the wall (Tedd, Chard, Charles & Symons, 1984; Powrie, 1985). Details of the revised pre-excavation lateral earth pressures are given in Table 2; the effect on the calculated soil stiffness profile is shown in Fig. 4.

This representation of wall installation is not ideal, as in practice the process will not be fully drained and will affect only the soil in the vicinity of the wall. However, the complete neglect of wall installation effects is also unlikely to be correct. Such effects will vary from case to case, and their quantification is a matter for engineering judgement: this is why the pre-excavation earth pressure coefficient is one of the factors investigated in this Paper.

FINITE ELEMENT MESH

The finite element mesh and the displacement boundary conditions are shown in Fig. 5. The idealized geometry is symmetrical about the centreline, so the mesh represents one half of a cross-section through the cutting. All deformations were assumed to occur in plane strain. The lower horizontal boundary to the analysis was set at the interface between the boulder clay and the rock, 40 m below original ground level (OGL). The far vertical boundary is sufficiently remote from the wall for changes in stress and strain to be negligible in practice. The soil and the wall were modelled generally using eight-noded quadrilateral elements, with smaller elements for the soil nearer the cutting, where changes in stress and strain were expected to be more significant.

Throughout the analysis, the line of zero gauge pore water pressure in the retained soil and the pore water pressure head at the outer vertical boundary were maintained at 1 m below OGL. The centreline of the cutting and the lower horizontal boundary were taken to be impermeable.

The concrete from which both the wall and the permanent prop are made was modelled as an impermeable elastic material with Young's modulus 17×10^3 MPa, Poisson's ratio 0·15, and unit weight 22 kN/m^3. This value of Young's modulus was adopted to take account of the possibility of long-term cracking and creep of the concrete. The wall elements were 1·5 m thick, giving a bending stiffness of $4{\cdot}78 \times 10^6$ kNm^2/m.

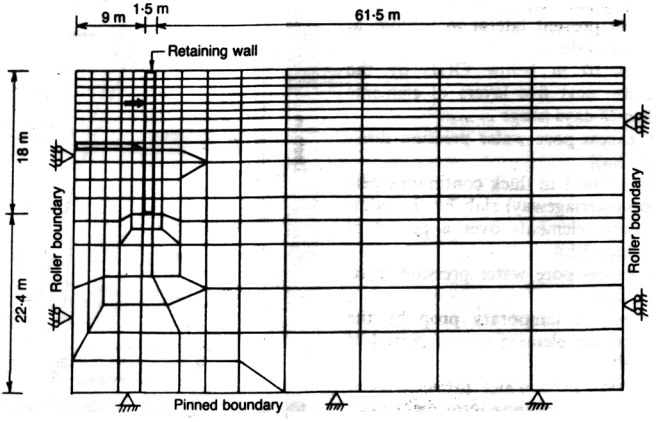

Fig. 5. Finite element mesh

The interface between the wall and the soil was modelled using slip elements having almost zero stiffness in tension, and an elastic shear modulus G of 7·5 MN/m^2 ($E' = 20$ MN/m^2 and $\nu' = 0{\cdot}2$) until a shear stress of tan 26° times the normal stress was reached, at which point the shear modulus was reduced by a factor of 100. The elastic modulus of the slip elements was chosen to correspond to the average pre-excavation stiffness of the soil over the depth of the wall. Ideally, it would have been better to have used slip elements whose elastic modulus was the same as that of the adjacent soil at any depth. However, because the slip elements are very thin (0·1 mm), and could equally well have been assigned the same stiffness as the wall, any error should be small. A further approximation was used in that the interface elements are not consolidation elements: this may lead to some error in the prediction of the onset of slippage, but should not significantly affect the behaviour of the bulk of the soil.

CONSTRUCTION SEQUENCE

The construction sequence modelled was, after installation of the wall, to excavate to a depth of 4 m below OGL; to install temporary props; to excavate to 1 m below final formation level (i.e. 10 m below OGL); to cast the continuous 1 m thick permanent prop slab; and finally to remove the temporary props. In the analysis, this sequence was simulated using the following steps (starting with the wall already in place)

(*a*) excavation to 4 m below OGL by the removal of the top four layers of elements over a period of 16 days (stage 1)
(*b*) construction of the (rigid) temporary prop over a period of one day by the addition of a bar element to prevent lateral movement at the appropriate node
(*c*) excavation to 10 m below OGL by the removal of the next five layers of elements over a further 28 days (stage 2)
(*d*) seven days' excess pore water pressure dissipation (stage 3(a))
(*e*) construction of the 1 m thick continuous permanent prop (carriageway) slab by the addition of concrete elements over a period of seven days (stage 3(b))
(*f*) seven days' excess pore water pressure dissipation (stage 3(c))
(*g*) dismantling of the temporary prop by the removal of the bar element over a period of 12 h (stage 3(d))
(*h*) 120 years' excess pore water pressure dissipation, modelling the long-term behaviour (stage 4).

During and after excavation, the pore water pressure at the excavated soil surface was set to zero. Throughout the analysis, changes in pore water pressure with time were calculated by the program in accordance with the drainage boundary conditions, the changes in boundary stresses resulting from excavation, and the specified permeability and consolidation characteristics of the soil.

The concrete in the slab was assumed to be incapable of sustaining structural stress resultants until after the end of stage 3(b). The connection between the wall and the permanent prop slab was modelled as a pinned joint (Fig. 5) at 10 m below OGL. As is shown below, the way in which this joint is constructed and/or modelled can have a significant effect on the bending moments in both the wall and the permanent prop slab.

The analysis was carried out in 47 increments. This was found to be sufficient to ensure satisfactory numerical accuracy: the use of 94 and 470 increments did not lead to any perceptible difference in the results.

RESULTS OF THE MAIN ANALYSIS (CASE 1)

Figure 6 shows the deflected profile of the wall at four instants during and after construction: *immediately after excavation to 4 m below OGL* (stage 1); immediately after excavation to 10 m below OGL (stage 2), immediately after removal of the temporary prop (stage 3) and 120 years after the end of construction (stage 4). Fig. 7

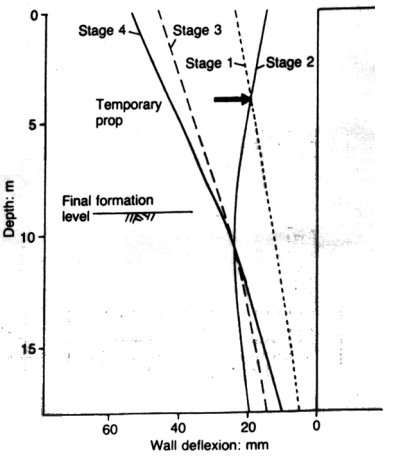

Fig. 6. Deflected wall profiles at various stages during and after construction

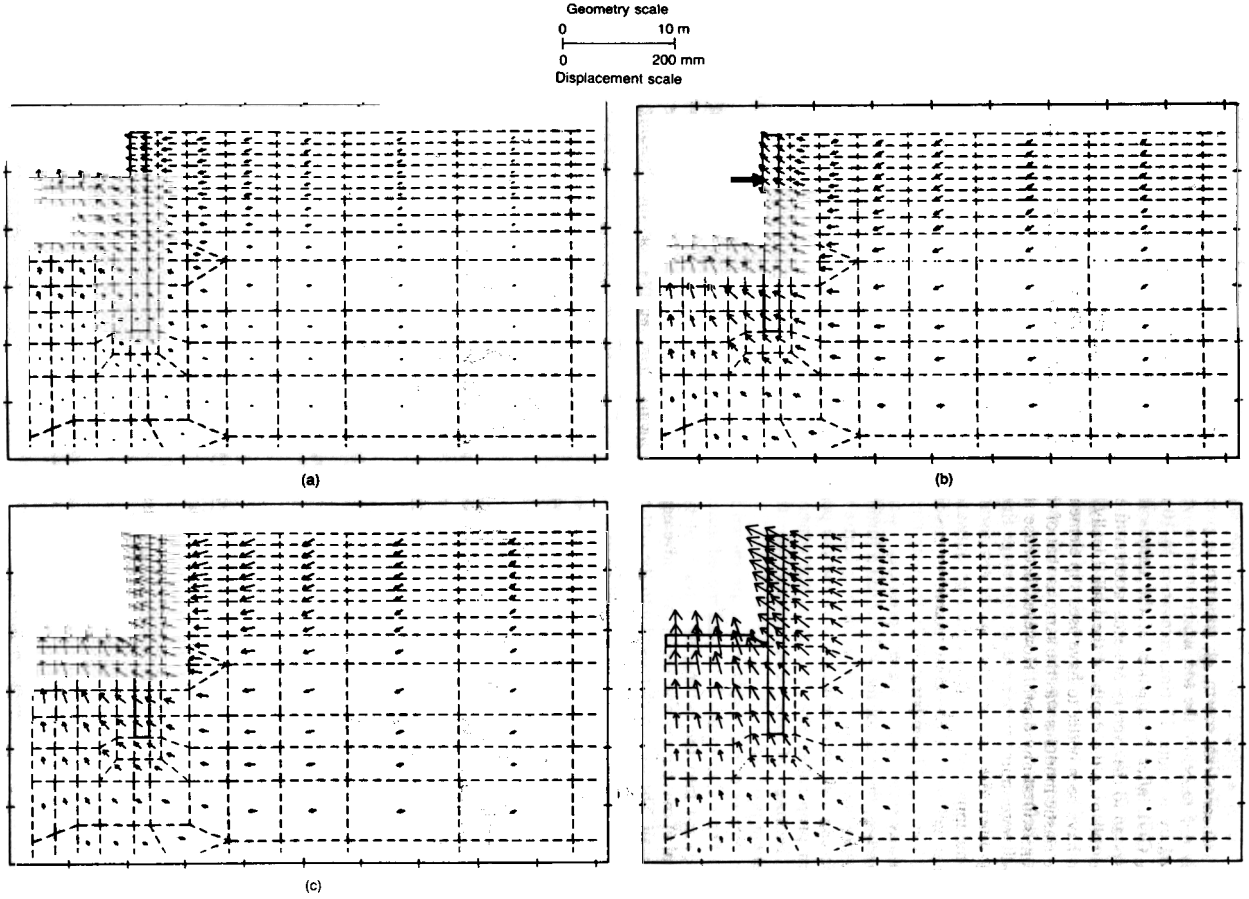

Fig. 7. Vectors of cumulative soil displacement: (a) stage 1; (b) stage 2; (c) stage 3; (d) stage 4

shows the vectors of cumulative soil movement at the same stages.

At the end of stage 1, deflexions were mainly the result of a rigid body rotation of the wall about an effective centre of rotation approximately 4–5 m below the toe, which itself moved forward by ~3 mm. During excavation to 10 m below OGL after installation of the temporary prop (stage 2), the toe of the wall continued to move forward, but the crest moved back into the retained soil as a result of the rotation of the wall about the temporary prop position. The effects of bending deformations on the deflected shape of the wall were more significant at this stage than at any other. After the removal of the temporary prop, the upper part of the wall moved outward, with the deflexion at the crest increasing rapidly from 15 mm to 47 mm (stage 3). In the long term, as steady-state pore water pressures were approached, the crest of the wall moved a further 8 mm into the excavation. The effective centre of the incremental rotation was just below the permanent prop rather than exactly at the connection, because of the compression of the permanent prop slab.

The vectors of soil displacement are shown in Fig. 7. The soil in front of the wall moved generally upward into the cutting, as a result of the removal of overburden and the inward movement of the wall. The soil which moved into the cutting during excavation to 10 m below OGL would in practice be removed. The long-term swelling of the excavated soil surface is partially restrained by the continuous permanent prop slab. During and immediately after excavation, the retained soil moved generally towards the cutting and slightly downward. In the long term, the analysis predicted an upward movement (heave) of the retained soil surface. This occurs as the shear deformations in the retained soil are dominated by elastic swelling of the underlying soil, as the stress relief due to excavation spreads perpendicular to the line of the wall. The stiffness of the soil in unloading may have been underestimated relative to the stiffness in shear, in which case this behaviour would not necessarily occur in practice. Also, the failure to model the stiffer response of a real soil when the change in stress is small (Jardine, Symes & Burland, 1984) will lead to the overestimation of the lateral extent of significant soil movement.

Figure 8 shows the distributions of lateral stress and pore water pressure at the end of stages 2–4. These are generally as would be expected. However, the lateral stresses are comparatively high just below the excavated soil surface, and low just below the retained soil surface, because (in contrast to the remainder of the mesh) the elements in these locations were at or approaching the yield surface.

Figure 9 shows wall bending moment diagrams at the end of each of stages 1–4. These were calculated directly from the stresses in the wall elements. The shapes of the bending moment diagrams are generally as would be expected, except perhaps for the negative bending moments of up to ~70 kNm/m in magnitude near the retained soil surface after the removal of the tem-

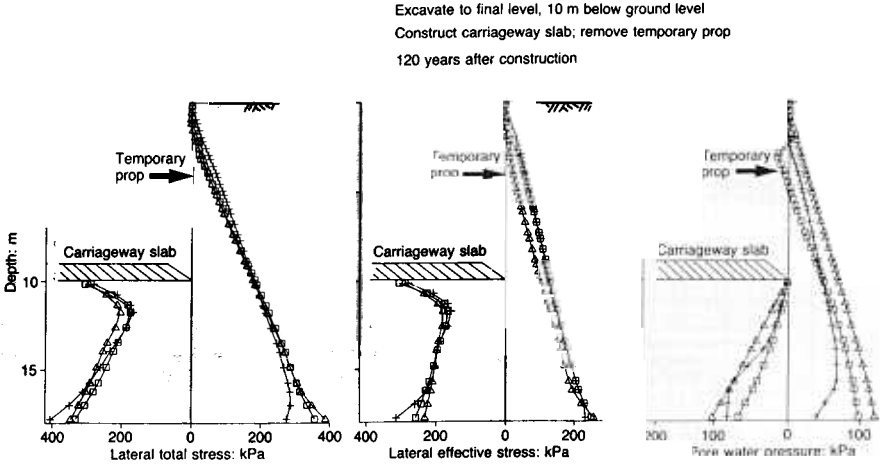

Fig. 8. Distributions of lateral stress and pore water pressure

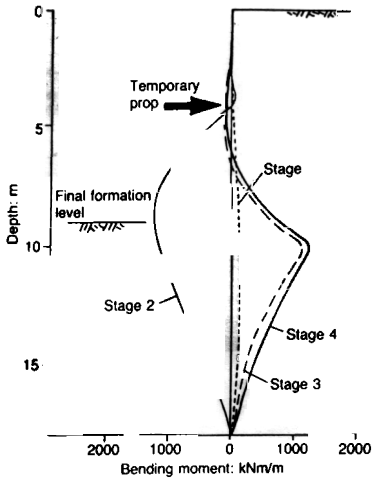

Fig. 9. Wall bending moments

porary prop. These may be due to the combined effects of shear stress on the wall and the low lateral stresses near the retained soil surface. Negative bending moments of a similar magnitude have been calculated in previous finite element analyses on unpropped cantilever walls (Fourie & Potts, 1989), for which the kinematics of deformation above formation level are similar; negative bending moments of up to 180 kNm/m in magnitude were measured in centrifuge tests on model walls propped at formation level retaining 10 m of overconsolidated kaolin (Powrie, 1986).

Figure 10 shows the development of axial thrust in both the temporary and permanent props, and the development of hogging bending moments in the permanent prop slab after placement of the concrete. The maximum permanent prop load occurs immediately after the temporary prop is removed. The expectation with in situ walls propped near the crest in overconsolidated clay is that the prop load will increase as the negative excess pore water pressures induced on excavation dissipate. For a wall propped at formation level, however, the long-term behaviour is not immediately obvious.

As the negative excess pore water pressures dissipate, the total stresses in front of the wall increase and, as a result of the restraint to swelling imposed by the continuous prop slab, the centroid of the total stress distribution rises (Fig. 8). Thus, the moment of the total stresses in front of the wall about the permanent prop increases less significantly than their resultant force. Behind the wall, there is only a small increase in total stress near the retained soil surface. The movement of

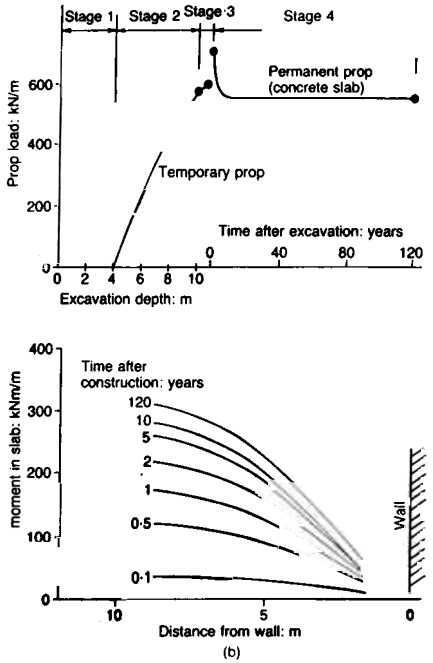

Fig. 10. (a) Development of prop loads; (b) development of bending moments in permanent prop slab

the centroid of the total stress distribution in front of the wall enables moment equilibrium to be maintained, even though the increase in total stress in front of the wall is greater than that behind. This results in a decrease in the axial thrust in the prop as long-term equilibrium conditions are approached.

Figure 8 shows that small variations in the stress distributions can cause comparatively large changes in the prop load. This sensitivity arises because bending moments and prop loads in cantilever walls derive from small differences between large quantities, which is why the reliable calculation of structural stress resultants for this type of wall in general is so difficult.

Figure 11 shows the stress paths followed by elements of soil at four locations around the wall: the stress ratios are generally well below the prescribed yield surface, except in the elements closest to the soil surfaces on either side of the wall.

CASE 2: INCREASED PRE-EXCAVATION LATERAL EARTH PRESSURES

An analysis was carried out in which the effects of wall installation were represented by a smaller

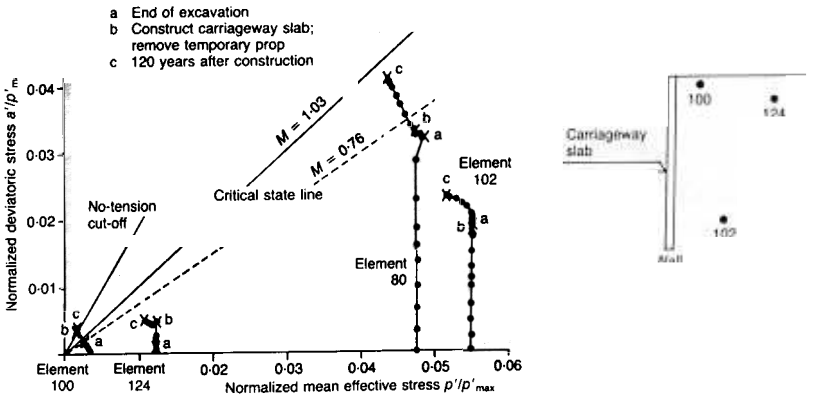

Fig. 11. Stress paths followed by four elements in the vicinity of the wall

reduction in lateral earth pressure coefficient above the toe, to 2·0 instead of 1·0. The assumed pre-excavation stress state in this case is given in Table 2.

The results of the case 2 analysis are summarized in Table 3 and Fig. 12. In general, the effects of the higher pre-excavation lateral earth pressures were

(*a*) to increase the outward deflexion of the crest of the wall by ~10%
(*b*) to increase the prop loads and wall bending moments by a factor of ~2
(*c*) to cause a slight increase in the permanent prop load as long-term equilibrium conditions were approached
(*d*) to reduce the bending moment and deflexion at the centre of the permanent prop slab by factors of approximately 2 and 1·5 respectively.

It is perhaps at first surprising that the increase in wall deflexion is not greater, and that the bending moments in and deflexions of the permanent prop slab are actually reduced. This is due to the increased soil stiffness (according to equations (1) and (2)) which results from the higher average effective stresses p' at all stages of the analysis. The increased pre-excavation soil stiffness profile is shown in Fig. 13. It is likely that the effects of an increased pre-excavation lateral earth pressure coefficient on soil and wall movements would have been more significant if a linear elastic soil model had been used.

The percentage increase in bending moments as long-term equilibrium conditions are approached is higher than in case 1. Because of the reduced scope for an increase in total stress in front of the wall, the resultant of the total stresses behind the wall increases by slightly more than the resultant of the total stresses in front, leading to a small increase in the prop load.

CASE 3: REDUCED SOIL STIFFNESS

In case 3, the value of the Cam clay parameter κ was increased to 0·032, as compared to 0·016 in case 1. This reduces the in situ soil stiffness at any depth by a factor of ~2, as shown in Fig. 13. The effect of this change was generally to increase displacements by a factor of almost 2, and maximum wall bending moments by up to ~15%, as shown in Table 3 and Fig. 12. It is clearly important that a reasonable estimate of the soil stiffness should be used in the analysis if realistic deformations are to be predicted. For a linear elastic/perfectly plastic soil model, the stiffness used in the analysis should perhaps be comparable with the measured secant stiffness at the appropriate shear strain. In the case of the Cam clay model, however, the stiffness of the soil changes as the analysis proceeds, so that it is more appropriate to compare the computed stiffness at the start of the analysis and the initial tangent modulus of the real soil.

CASE 4: REDUCED WALL THICKNESS

In this analysis, the thickness of the wall was reduced from 1·5 m to 1·25 m, decreasing the bending stiffness of the wall by about 40%. The principal effects of this change were

(*a*) to increase the long-term deflexion at the crest of the wall by ~15%
(*b*) to reduce the load in the permanent prop by ~15% and the maximum wall bending

Table 3. Summary of results for cases 1–7

	Case 1: standard			Case 2: increased pre-excavation K			Case 3: reduced soil stiffness			Case 4: reduced wall thickness			Case 5: reduced slab thickness			Case 6: reduced temporary prop stiffness			Case 7: rigid connection		
Stage	2	3	4	2	3	4	2	3	4	2	3	4	2	3	4	2	3	4	2	3	4
Outward deflexion at crest of wall: mm	14·9	46·4	54·6	10·3	51·3	60·5	31·3	76·9	90·2	13·9	52·6	62·8	15·7	42·1	48·9	17·6	47·7	55·9	14·9	41·1	44·8
Outward deflexion at toe of wall: mm	19·6	14·6	10·4	16·7	11·6	8·5	39·4	27·8	19·3	18·9	14·6	10·6	18·4	14·6	10·7	19·5	14·6	10·6	19·6	14·7	11·4
Outward deflexion at temp. prop position: mm	19·5	38·0	43·0	15·6	39·9	45·2	37·3	64·1	72·3	20·1	42·5	48·6	19·5	34·7	38·9	21·5	39·1	44·0	19·5	34·2	36·1
Outward deflexion at formation level: mm	24·1	25·1	25·6	20·8	22·4	22·8	43·7	44·9	45·7	25·9	26·7	27·2	23·1	24·4	24·7	24·9	25·9	26·3	24·1	24·5	24·3
Approximate maximum wall bending moment: kNm/m	−1260	1151	1245	−1558	1998	2370	−1445	1421	1345	−1075	963	1113	−1102	1027	1114	−1208	1100	1213	−1260	846	930
Load in temporary prop: kN/m	582	—	—	953	—	—	651	—	—	555	—	—	545	—	—	553	—	—	582	—	—
Load in permanent prop (carriageway slab): kN/m	—	716	558	—	1075	1087	—	707	548	—	534	471	—	709	564	—	676	538	—	722	612
Maximum hogging bending moment in permanent prop: kNm/m	—	—	309	—	—	146	—	—	531	—	—	280	—	—	59	—	—	301	—	—	212*
Post-construction heave at centre of carriageway slab: mm	—	—	20·6	—	—	14·2	—	—	38·3	—	—	19·8	—	—	23·9	—	—	20·3	—	—	17·3
Post-construction heave at edge of carriageway slab: mm	—	—	13·6	—	—	10·8	—	—	26·4	—	—	13·2	—	—	12·2	—	—	13·4	—	—	13·2

* Sagging moment of 171 kNm/m near the wall.

Case	Prop load: kN/m	
	Temporary	Permanent
1	582	558
2	953	1087
3	651	548
4	555	471

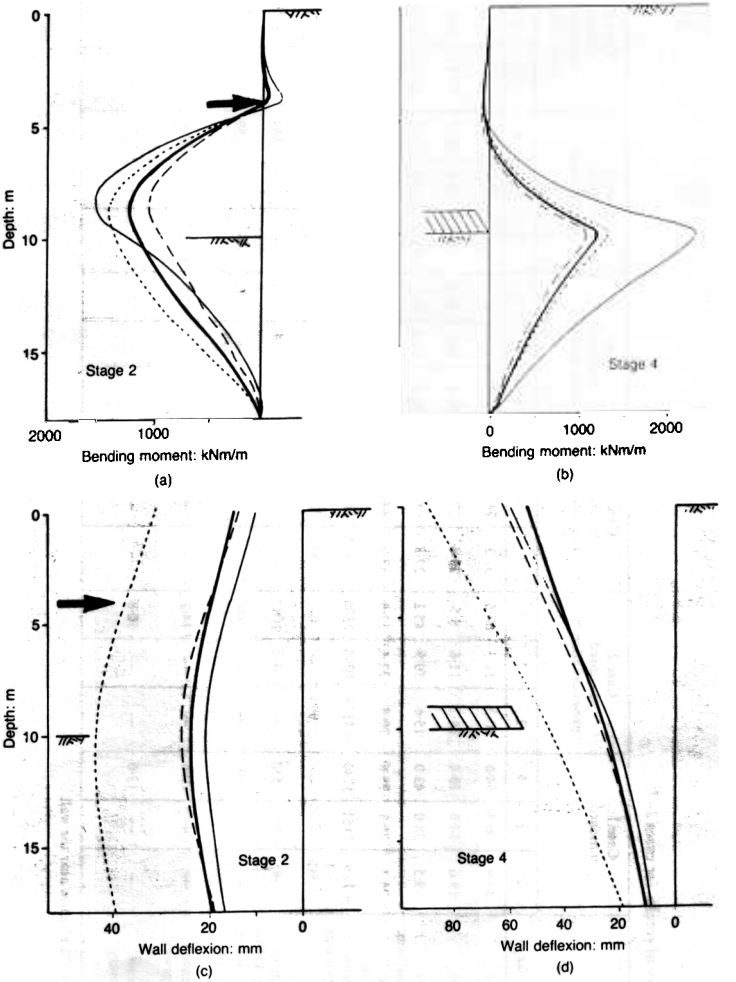

Fig. 12. Cases 1–4: comparison of: (a), (b) wall bending moments; (c), (d) wall movements

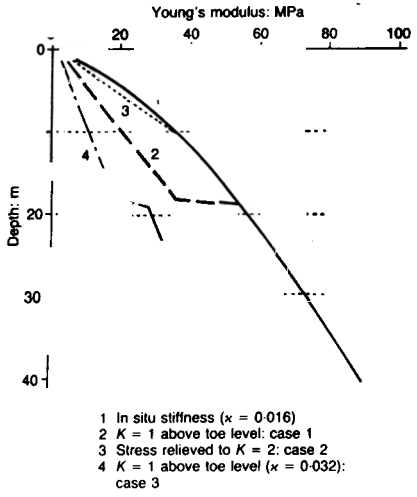

Fig. 13. Modified soil stiffness profiles, cases 2 and 3

moment by ~10% (both at 120 years after construction).

It is not surprising that reducing the wall thickness from 1·5 m to 1·25 m has little effect, as in both cases the wall is very stiff in comparison with the soil it supports. Soil–wall stiffness can be characterized by the dimensionless group $R = G^*H^4/EI$ where H is the overall height of the wall, EI is its bending stiffness per metre run, and G^* is the rate of increase of soil shear modulus with depth. With $K = 1$ immediately before excavation, the rate of increase in Young's modulus E' with depth is $\sim 2 \times 10^3$ kPa/m (Fig. 13, profile 2). For Poisson's ratio $\nu' = 0{\cdot}2$, $G^* = 0{\cdot}83 \times 10^3$ kPa/m. For the wall of thickness 1·5 m, $EI = 4{\cdot}78 \times 10^6$ kNm^2/m, giving $R = 18{\cdot}3$ for $H = 18$ m. For the wall of thickness 1·25 m, $EI = 2{\cdot}77 \times 10^6$ kNm^2/m and $R = 31{\cdot}5$. Conventionally, walls with R less than ~400 are regarded as stiff (Bolton, Powrie & Symons, 1989).

CASE 5: REDUCED PERMANENT PROP SLAB THICKNESS

In this case the thickness of the carriageway slab was reduced from 1 m to 0·5 m. The bending moment at the centre of the slab was reduced by a factor of ~5, whereas the heave at this location was increased by only ~20%. However, the differential deflexion (between the edges and the centre of the carriageway) was increased by 70% from 7 mm to 11·7 mm. This is consistent with the combined effects of the decrease in moment by a factor of 5 and the decrease in bending stiffness by a factor of 8, which for a uniformly loaded simply supported beam would lead to an increase of 60% in the central deflexion.

With the thickness of the permanent prop slab reduced, the movement of the crest of the wall after placement of the permanent prop was generally smaller. During excavation to the level of the underside of the carriageway slab, the reduction in the excavated depth from 10 m to 9·5 m increased the embedment ratio (i.e. the depth of embedment/retained height) from 0·8 to 0·9, reducing the magnitude of rigid body rotation about the temporary prop. In the long term, deformations due to rotation were again reduced because the pinned connection between the permanent prop slab and the wall was at a depth of 9·5 m below OGL, rather than at 10 m below OGL as in case 1. The reduced excavation depth was probably also responsible for the small decrease in the long-term heave at the edge of the carriageway slab (from 13·6 mm to 12·2 mm). The results of this analysis are summarized in Table 3 and Fig. 14.

CASE 6: REDUCED TEMPORARY PROP STIFFNESS

In the main analysis (case 1), the temporary prop was assumed to be rigid. Under the load of 600 kN/m predicted by the main analysis, real props spanning the entire width of the excavation fabricated from 600 mm dia., 12·5 mm thick, circular hollow steel sections at intervals of 2 m along the line of the wall would be expected to shorten by approximately 4 mm. In order to investigate the importance of any stress relief in the retained soil which this might cause, an analysis was carried out with a temporary prop stiffness appropriate to the arrangement described above, $P/\delta = EA/L = 2{\cdot}8 \times 10^5$ kN/m. The effects of prestressing or lack of fit, which may occur in practice and could in principle be taken into account for a given design situation, were not considered.

The results summarized in Table 3 and Fig. 14 show that although the outward deflexion at the crest of the wall during construction was increased by almost 20%, the effect of this change in the long term was insignificant in practice.

CASE 7: THE CONSTRUCTION JOINT BETWEEN THE WALL AND THE PERMANENT PROP SLAB

In the main analysis, a triangular element was used at the end of the permanent prop slab to reduce the moment-carrying capacity of the connection to the wall (Fig. 15). In reality, the axial thrust carried by the permanent prop would

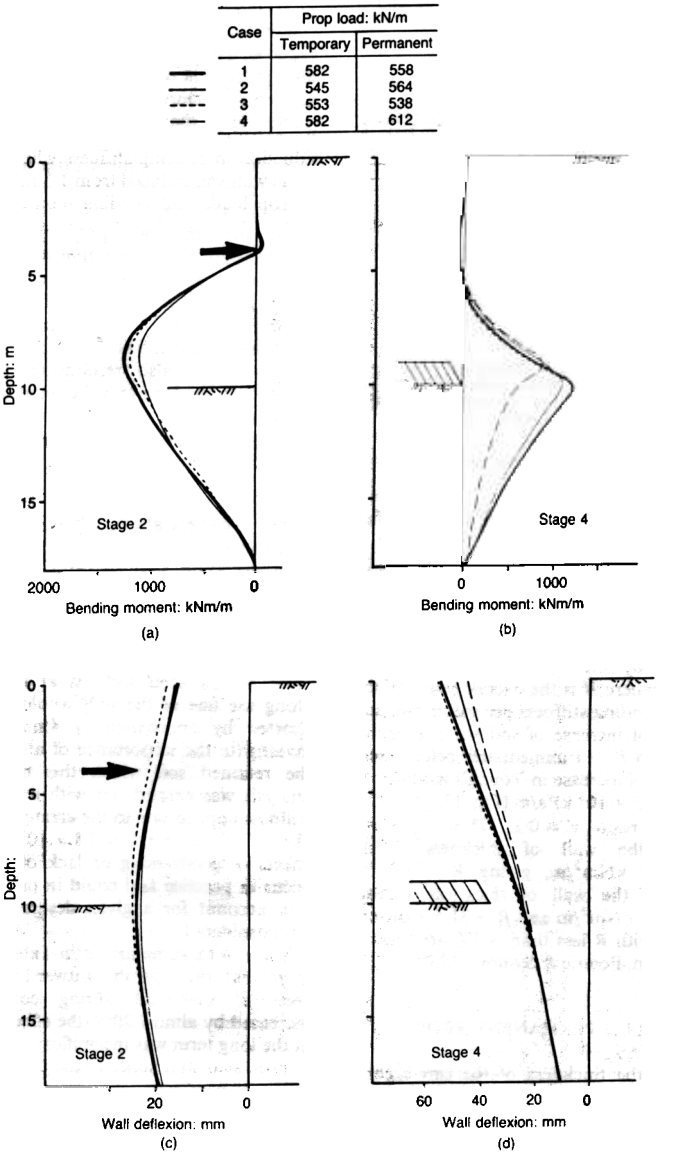

Fig. 14. Cases 5–7: comparison of: (a), (b) wall bending moments; (c), (d) wall movements

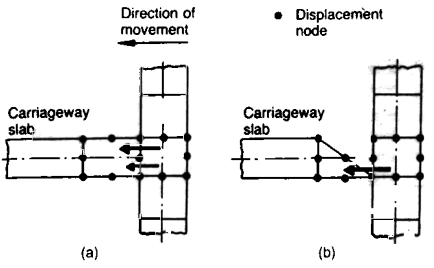

Fig. 15. Detail of joint between wall and permanent slab: (a) rigid connection; (b) pinned connection

enable a butted joint to transmit bending moments, provided that the interface remained in compression. The provision of an effectively rigid joint would generate sagging moments in the slab where it meets the wall. This would in turn result in a reduction in the hogging moment at the centre of the slab and reduce the magnitudes of the bending moments in the wall itself.

In order to investigate the effect of a more rigid connection (case 7), the triangular element at the end of the permanent prop slab was replaced by a quadrilateral element (Fig. 15). An interface element between the two members was used to prevent the transmission of tensile stress, effectively simulating a butted joint. However, the interface remained in compression throughout the analysis due to the tendency of the wall to move forward into the excavation. The principal effects of this change in the long term (i.e. after 120 years) were

(*a*) to induce a sagging moment of 171 kNm/m at the end of the permanent prop slab near the wall
(*b*) to reduce the maximum hogging moment in the centre of the slab from the case 1 value of 309 kNm/m to 212 kNm/m
(*c*) to reduce the maximum wall bending moment from 1245 kNm/m to 930 kNm/m.

The provision of an effectively bending-stiff connection enables the permanent prop slab to act to some extent as a relieving platform, with the reduction in wall bending moments resulting from upward pressure on a platform in front of the wall instead of downward pressure on a conventional platform behind. A further advantage of a butted joint is that it would be much simpler to construct in practice than a true pinned connection.

CONCLUSION

The importance of the soil stiffness and the assumed pre-excavation lateral earth pressures on the behaviour of the wall cannot be overemphasized. The structure investigated in this analysis was very stiff, so that the magnitude of soil and wall movements was governed by the stiffness of the soil rather than that of the wall. A reduction in the soil stiffness by a factor of 2 resulted in an increase in wall movement of almost the same magnitude. Conversely, wall movements were little affected by a 40% reduction in bending stiffness when the thickness of the wall was reduced from 1·5 m to 1·25 m.

Prop loads and bending moments are dependent on the assumed pre-excavation lateral earth pressures. Although an increase in pre-excavation lateral stresses did not increase the computed wall movements significantly, this was due to the accompanying increase in soil stiffness for the soil model used in this analysis.

The detail of the permanent prop slab may also be important. If the thickness of the slab can be reduced, there will be a general reduction in the magnitude of wall movements simply because (if the total length of the wall remains the same) the embedment ratio is increased. The provision of a quasi-rigid construction joint between the permanent prop slab and the wall will reduce bending moments in the wall and the hogging moment at the centre of the prop slab, but will introduce a sagging moment in the slab at the connection to the wall. Even a butted joint may have this effect, provided that the interface between the two members remains in compression.

In addition to the factors investigated in this Paper, the behaviour of the structure might be affected by any or all of the following.

(*a*) Leakage of groundwater through the wall might raise the long-term pore water pressures in front of the wall below formation level, leading to an increased tendency of the soil to swell.
(*b*) If the permeability of the soil has been overestimated, the rate of dissipation of negative excess pore water pressure and hence the heave which occurs during construction will have been overpredicted. This will in turn result in an overestimate of the volume of soil removed in trimming the excavated soil surface before placement of the permanent prop slab, and hence in the underprediction of the eventual upthrust and/or post-construction heave. Perhaps more seriously, the underestimation of the effective soil permeability might lead to the underprediction of movements during excavation to formation level with the temporary props in place, because of the increased rate of dissipation of negative excess pore water pressures at this stage.

(c) In the analysis, the pore water pressure at the excavated soil surface was set to zero during and after construction. In effect, this surface has been assumed to act as a recharge boundary while the pore water pressures below it are negative. In reality this may not be so, in which case the rate of dissipation of negative excess pore water pressure and heave during construction will have been overpredicted, leading again to the underprediction of the eventual upthrust on, and/or the post-construction heave of, the permanent prop slab. Note also that it was assumed in the analysis that drainage underneath the carriageway slab will maintain zero pore water pressures at the excavated soil surface in the long term.

ACNOWLEDGEMENTS

The Authors are grateful to Dr A. M. Britto for his advice and helpful comments, and to the Croucher Foundation for its provision of financial support to Dr Li.

NOTATION

e void ratio
e_0 void ratio on critical state line at $p' = 1$ kPa
E Young's modulus
E' effective stress Young's modulus
EI flexural rigidity
G shear modulus
G^* rate of increase of shear modulus with depth
H overall height of retaining wall
I second moment of cross-sectional area
k (with subscript to denote direction) permeability
K bulk modulus
K earth pressure coefficient
K_0 initial in situ (at rest) earth pressure coefficient
K_p passive earth pressure coefficient
M slope of critical state line in $q : p'$ space
p' average effective stress $= (\sigma_1' + \sigma_2' + \sigma_3')/3$
q deviatoric stress invariant
R soil/wall stiffness ratio G^*H^4/EI
S slope of no-tension cut-off in $q : p'$ space
v specific volume
γ unit weight of soil
γ_w unit weight of water
Γ specific volume on critical state line at $p' = 1$ kPa
κ slope of unload/reload lines in $v : \ln p'$ space
λ slope of critical state line in $v : \ln p'$ space
ν' effective stress Poisson's ratio
σ' normal effective stress
τ shear stress
ϕ' angle of shearing
ϕ_H angle of Hvorslev surface

Subscript
h horizontal
u undrained
v vertical

REFERENCES

Bolton, M. D., Britto, A. M., Powrie, W. & White, T. P. (1989). Finite element analysis of a centrifuge model of a retaining wall embedded in a heavily overconsolidated clay. *Comput. Geotech.* **7**, 289–318.

Bolton, M. D., Powrie, W. & Symons, I. F. (1989). The design of stiff in situ walls retaining overconsolidated clay. Part 1: short term behaviour. *Ground Engng* **22**, No. 8, 44–48.

Britto, A. M. & Gunn, M. J. (1987). *Critical state soil mechanics via finite elements.* Chichester: Ellis Horwood.

Fourie, A. B. & Potts, D. M. (1989). Comparison of finite element and limiting equilibrium analyses for an embedded cantilever retaining wall. *Géotechnique* **39**, No. 2, 175–188.

Jardine, R. J., Symes, M. J. & Burland, J. B. (1984). Measurement of soil stiffness in the triaxial apparatus. *Géotechnique* **34**, No. 3, 323–340.

Li, E. S. F. (1990). *On the analysis of singly-propped diaphragm walls.* PhD thesis, University of London.

Mayne, P. W. & Kulhawy, F. M. (1982). K_0-OCR relationships in soils. *J. Geotech. Engng Div., Am. Soc. Civ. Engrs* **108**, No. 6, 851–872.

Powrie, W. (1985). Discussion on performance of propped and cantilevered rigid walls. *Géotechnique* **35**, No. 4, 546–548.

Powrie, W. (1986). *The behaviour of diaphragm walls in clay.* PhD thesis, University of Cambridge.

Schofield, A. N. (1980). Cambridge geotechnical centrifuge operations. *Géotechnique* **20**, No. 2, 129–170.

Stroud, M. A. & Butler, F. G. (1975). The standard penetration test and the engineering properties of glacial materials. *The engineering behaviour of glacial materials*, pp. 117–128. Birmingham: Midland Soil Mechanics and Foundation Engineering Society.

Symons, I. F. & Carder, D. R. (1989). Long term behaviour of embedded retaining walls in overconsolidated clay. *Instrumentation in geotechnical engineering*, pp. 155–173. London: Thomas Telford.

Tedd, P., Chard, B. M., Charles, J. A. & Symons, I. F. (1984). Behaviour of a propped embedded retaining wall in stiff clay at Bell Common tunnel. *Géotechnique* **34**, No. 4, 513–532.